

Facile synthesis of wurtzite copper–zinc–tin sulfide nanocrystals from plasmonic djurleite nuclei†

Cite this: *J. Mater. Chem. A*, 2013, **1**, 337

Hsueh-Chung Liao,^a Meng-Huan Jao,^a Jing-Jong Shyue,^b Yang-Fang Chen^c and Wei-Fang Su^{*a}

The present research demonstrates a facile one-pot heating process without injection to synthesize an important light harvesting quaternary nanocrystal: wurtzite copper–zinc–tin sulfide (w-CZTS). High quality w-CZTS nanocrystals can be easily obtained by mixing all the precursors and simply heating to the reaction temperature. The nano-crystal formation mechanism is thoroughly investigated and resolved by X-ray diffraction spectroscopy (XRD), transmission electron microscopy (TEM) and electron energy loss spectroscopy (EELS). It starts with the nucleation of plasmonic djurleite $\text{Cu}_{1.94}\text{S}$, subsequent growth of CZTS– $\text{Cu}_{1.94}\text{S}$ heterostructures and inter-diffusion of cations and then finally leads to single phase and single crystal w-CZTS nanocrystals. The mechanism of nanocrystal formation can be applied universally regardless of the type of zinc and tin precursor for high quality w-CZTS nanocrystals. The in-depth interpretations of the reaction mechanism of this process significantly advance the current knowledge of multi-component nanocrystal formation. The developed method is scalable for high throughput and low cost w-CZTS suspensions which await practical photovoltaic applications.

Received 31st August 2012

Accepted 11th October 2012

DOI: 10.1039/c2ta00151a

www.rsc.org/MaterialsA

Introduction

Nanocrystals have been extensively investigated over the last two decades from their fundamental science to their practical applications. There is no end to the quest for a facile synthesis of high quality colloidal nanocrystals with controlled shape, size, composition and crystal structure. This generally involves precise control of the formation of the nanocrystals, *i.e.* nucleation, growth, size focusing and ripening.^{1,2} The hot injection strategy is typically adopted which results in sudden high level supersaturation.^{1,3–6} This leads to a simultaneous burst of nucleation and well-controlled growth and thus high quality nanocrystals. However, such a method has limitations in terms of the reproducibility and large scale production. An alternative heating (or non-injection) route was hence demonstrated for more convenient control by mixing all the precursors together and simply heating them.^{1,7–11} Nonetheless, the control of the reactivity of the precursors during the heating process needs to be addressed. A successful strategy has been reported by synthesizing organometallic precursors such as metal oleate or metal diethyldithiocarbamate complexes with controlled

thermal pyrolysis occurring during the heating process.^{7,12–14} However, this requires multiple-pot reactions and furthermore has limitations in the preparation of the multi-component nanocrystals due to the different thermal decomposition temperatures among the organometallic precursors.

Considering the copper–zinc–tin sulfide (CZTS) quaternary nanocrystal, it was recently discovered that it is an important material for photovoltaics owing to the advantages of its optimal band gap, earth-abundant and nontoxic components, high absorption coefficient, *etc.* obtained through a low cost wet-chemistry process.^{15–19} However, with such complicated multi-component quaternary nanocrystals there is a challenge in adopting a convenient one-pot heating process. Namely, either using common cationic precursors (metal acetate, metal chloride, *etc.*) or organometallic precursors (metal-oleate, metal-diethyldithiocarbamate, *etc.*), the different reactivities or different thermal decomposition temperatures among the precursors should be taken into account to avoid the formation of additional phases such as copper sulfide, tin sulfide or zinc sulfide. Herein, we present a facile one-pot heating synthesis of wurtzite based CZTS (w-CZTS) nanocrystals for the first time, which is belong to the orthorhombic crystal system. This is a newly discovered crystal structure of CZTS rather than the typically reported zinc blende (tetragonal) structure that has recently attracted great attention for sustainable energy applications.^{20–25} Lu *et al.* reported the synthesis of wurtzite $\text{Cu}_2\text{ZnSnS}_4$ nanocrystals for the first time.²⁰ However, the relatively broad size distribution and the adoption of the hot injection method would limit it in further scaling up and

^aDepartment of Materials Science and Engineering, National Taiwan University, No. 1, Sec. 4, Roosevelt Road, Taipei 10617, Taiwan. E-mail: suwf@ntu.edu.tw; Fax: +886 2 33664078; Tel: +886 2 33664078

^bAcademia Sinica, No. 128, Academia Road, Section 2, Nankang, Taipei 115, Taiwan

^cDepartment of Physics, National Taiwan University, No. 1, Sec. 4, Roosevelt Road, Taipei 10617, Taiwan

† Electronic supplementary information (ESI) available: Simulated XRD pattern of w-CZTS. See DOI: 10.1039/c2ta00151a

practical applications. This work demonstrates a simple one-pot heating process to prepare w-CZTS nanocrystal suspensions. The mechanism of nanocrystal formation is systematically studied by optical characterization, powder X-ray diffraction (XRD) and TEM analysis. Electron energy loss spectroscopy (EELS) was further employed to examine the elemental spatial distributions and thus determine the composition uniformity. The types of zinc and tin cation precursors in the synthesis were varied to support the proposed mechanism for overcoming the typical challenge of balancing cation reactivity in preparing multi-component nanocrystals through a one-pot heating reaction.

Experimental details

Nanocrystals synthesis

Copper(II) acetylacetonate ($\text{Cu}(\text{acac})_2$, Aldrich, 99.99%), zinc acetate dehydrate ($\text{Zn}(\text{OAc})_2$, ACROS, 98%), zinc chloride (ZnCl_2 , ACROS, 98%), tin(II) chloride dehydrate (SnCl_2 , Aldrich, 99.995%), tin(II) acetate ($\text{Sn}(\text{OAc})_2$, Aldrich, 99.995%), *n*-dodecanethiol (ACROS, 98%), and oleylamine (ACROS, C-18 content 70–80%) were purchased and used as received without further purification. All the syntheses were carried out using a Schlenk line. In a typical synthesis, a mixture of 1 mmol $\text{Cu}(\text{acac})_2$, 0.5 mmol $\text{Zn}(\text{OAc})_2$, 0.5 mmol SnCl_2 , 1 g *n*-dodecanethiol, and 12 g oleylamine was added to a 25 mL three-neck-flask and heated under vacuum to 60 °C for 60 min. Then the mixture was heated up to the reaction temperature, *i.e.* 200 °C, 230 °C, or 260 °C, under an Ar flow. When the temperature reached 130 °C, the color of the mixture changed from turbid white to transparent yellow. The reaction mixture was kept at the reaction temperature for different reaction times. After the reaction had finished, the flask was removed from the heating mantle and allowed to naturally cool to room temperature. For purification, the nanocrystals were precipitated from the reaction mixture by adding 15 mL of isopropanol and then centrifuged at 8000 r.p.m. for 10 min to remove some unreacted chemicals and byproducts. Finally the nanocrystals could be redispersed well in a nonpolar solvent such as hexane, toluene, or chloroform. For the synthesis employing different cationic precursors, *i.e.* $\text{Zn}(\text{OAc})_2$ and $\text{Sn}(\text{OAc})_2$ or ZnCl_2 and SnCl_2 , all the processes were performed identically according to the above description.

Characterization

For the TEM and EELS characterization, a drop of the nanocrystal suspension in toluene was dried on a 200 mesh carbon-membrane-coated copper grid. The TEM images were obtained by using an FEI Tecnai G2 T20 microscope operating at 200 keV. The EELS mapping was carried out using a post-column energy filter (Tridium, Gatan) on a JEOL JEM-2100F. The powder XRD was performed using an X-ray diffractometer (PANalytical X'Pert PRO) with filtered $\text{Cu K}\alpha$ radiation ($\lambda = 1.54 \text{ \AA}$). The absorption spectra were measured using a Hitachi U-4100 optical spectrometer. The simulation of the w-CZTS XRD patterns was conducted using Diamond 3.2 software (see ESI†).

Results and discussion

We first used copper acetylacetonate, zinc acetate and tin chloride as the precursors of Cu, Zn and Sn respectively in a molar ratio of 2 : 1 : 1. Oleylamine and dodecanethiol were used as the surface ligand and anion precursor respectively. All the chemicals were mixed under an argon flow and simply heated up to the reaction temperature (see the experimental method for details). Fig. 1a shows the XRD patterns of the synthesized nanocrystals after reaction at 200 °C, 230 °C and 260 °C for 1 hour. For the reaction temperature of 260 °C, the diffraction peaks exhibit the features of the pure wurtzite crystal structure which has hexagonal closely packed sulfur anions with cations in the interstices. The corresponding planes are indexed according to simulated wurtzite patterns (ESI†). When the nanocrystals were synthesized at 200 °C and 230 °C, however, there are some additional diffraction peaks at 37.6°, 48.7°, *etc.* These peaks can be attributed to the copper sulfide because the dodecanethiol as a soft Lewis base reacts preferentially with the Cu^+ as a soft Lewis acid following the soft-soft acid-base model.²⁶ Plasmonic optical absorption can be used to characterize the composition of the copper sulfide as shown in Fig. 1b. The three nanocrystals synthesized at different temperatures exhibit optical absorbance in the visible light region which corresponds to the band gap transition of the semiconductor. However, the nanocrystals synthesized at 200 °C and 230 °C both show an obvious broad absorption peak in the near-infrared region. This results from the localized surface plasmonic resonance (LSPR) of the copper sulfide phase with deficient copper and thus excess free carriers.^{27,28} According to the dipole surface plasmon, the LSPR frequency (ω_{sp}) can be expressed as:²⁹

$$\omega_{\text{sp}} = \sqrt{\frac{\omega_{\text{p}}^2}{1 + 2\epsilon_{\text{m}}} - \gamma^2} \quad (1)$$

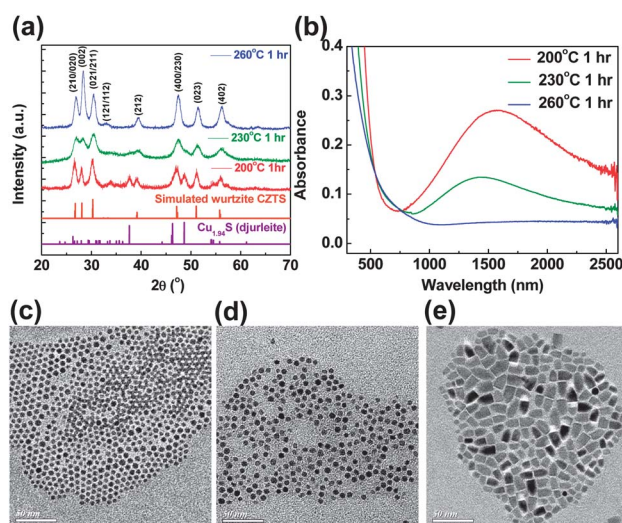


Fig. 1 (a) XRD patterns and (b) absorption spectra of different nanocrystals obtained after the reaction at different temperatures for 1 hour. (c–e) TEM images of different nanocrystals obtained after the reaction at 200 °C, 230 °C, and 260 °C for 1 hour respectively.

where ϵ_m is the dielectric constant of the solvent, ω_p is the plasma frequency of free electron gas and γ is the collision frequency. The absorption spectrum of the nanocrystals synthesized at 200 °C (Fig. 1b) for 1 hour exhibits a clear LSPR in the near infrared region which is centered at ~ 1520 nm, indicating an LSPR frequency of 0.82 eV. The bandwidth of the absorbance implies that γ is 0.29 eV and that the dielectric constant of the tetrachloroethylene solvent $\epsilon_m = 2.28$. As a result, ω_p is determined to be 2.05 eV, which can be used to calculate the free carrier density:

$$\omega_p = \sqrt{\frac{N_h e^2}{\epsilon_0 m_h}} \quad (2)$$

where m_h is the effective hole mass which is approximately 0.8 times the mass of an electron. N_h is the free carrier density. Therefore, the copper deficiency can be determined to be 5.7%, indicating a composition of $\text{Cu}_{1.94}\text{S}$ (djurleite). A similar concentration of $\sim 6\%$ was obtained from the plasmonic absorption of the nanocrystals synthesized at 230 °C for 1 hour. Therefore, the obtained nanocrystals synthesized at 200 °C and 230 °C are indeed $\text{Cu}_{1.94}\text{S}$ -CZTS heterostructures. The reference pattern of $\text{Cu}_{1.94}\text{S}$ (JCPDS no. 23-0959) shown in Fig. 1a further provides evidence which reveals identical diffraction peaks at 37.6°, 48.7°, etc. to those in the $\text{Cu}_{1.94}\text{S}$ -CZTS heterostructures. This kind of heterostructure composed of copper sulfide and other metal sulfides has also been observed in other materials because the preferential reaction between Cu^+ and S^{2-} makes copper sulfide a general starting phase.³⁰⁻³⁴ Following the nucleation of copper sulfide, the arrangement of the S^{2-} anions serving as the backbone enables the subsequent growth of other metal sulfides based on the same anion arrangement structure. The $\text{Cu}_{1.94}\text{S}$ phase has a hexagonally packed backbone of S^{2-} and formed preferentially during heating. The w-CZTS which also has hexagonally packed S^{2-} hence forms subsequently. It is noteworthy that the final products reported in similar nanocrystal formation processes are typically copper sulfide-metal sulfide heterostructures which consist of both a starting phase (copper sulfide) and a multi-component phase (metal sulfide).³¹⁻³⁴ However, it is found that the present case is distinctively different in that the starting phase $\text{Cu}_{1.94}\text{S}$ can be expelled and thus the pristine CZTS phase can be obtained. Namely, at elevated reaction temperatures, the $\text{Cu}_{1.94}\text{S}$ starting phase tends to diminish as indicated by the decreased diffraction intensity of $\text{Cu}_{1.94}\text{S}$ (Fig. 1a) and decreased plasmonic absorption (Fig. 1b). We speculate that the $\text{Cu}_{1.94}\text{S}$ -CZTS heterostructures have extremely high mobility of cations and a high concentration of vacancies due to the presence of the plasmonic features. Both characteristics facilitate the interdiffusion of free cations analogous to a fluid that flow around the sulfur anions. The higher reaction temperature hence provides more energy to overcome the energy barrier to interdiffusion that results from the different atomic sizes and thus expel the starting phase $\text{Cu}_{1.94}\text{S}$. Fig. 1c-e show the corresponding transmission electron microscopy images of the nanocrystals synthesized at 200 °C, 230 °C and 260 °C respectively. The $\text{Cu}_{1.94}\text{S}$ -CZTS heterostructures (Fig. 1c-d) reveal

nanoparticles with diameters of 6 nm and moderate size uniformity. On the other hand, the pristine w-CZTS (Fig. 1e) exhibits bullet shapes or leaf shapes with dimensions of 14 nm and a size distribution (σ_r) of 28%. The size distribution is relatively broad because of the short reaction time and can be narrowed by a size focusing effect (discussed later).

In order to further clarify the nanocrystal formation process, we examined the nanocrystals synthesized at 230 °C for different times, *i.e.* 30 minutes, 1 hour, 2 hours, 4 hours, 8 hours, 16 hours and 24 hours. Fig. 2 shows the XRD patterns of these nanocrystals. When the reaction time is 4 hours or longer, all of the patterns reveal the pristine wurtzite crystal structure. Further increasing the reaction time leads to an increased diffraction intensity of the (002) plane peak which indicates the preferred orientation and anisotropic shape of the synthesized nanocrystals. On the other hand, discernible diffractions resulting from $\text{Cu}_{1.94}\text{S}$ are observed at the beginning of the reaction (30 minutes and 1 hour) which again suggests the $\text{Cu}_{1.94}\text{S}$ as the starting phase. The XRD results imply that extending the reaction time can also provide sufficient energy for cation inter-diffusion and hence expel the starting phase $\text{Cu}_{1.94}\text{S}$. Furthermore, the phase transformation from the $\text{Cu}_{1.94}\text{S}$ -CZTS heterostructure to the pristine w-CZTS is completed after reacting for 4 hours.

Fig. 3a-g show the corresponding TEM images of the nanocrystals synthesized for different reaction times. They present similarly monodispersed nanoparticles with the $\text{Cu}_{1.94}\text{S}$ -CZTS

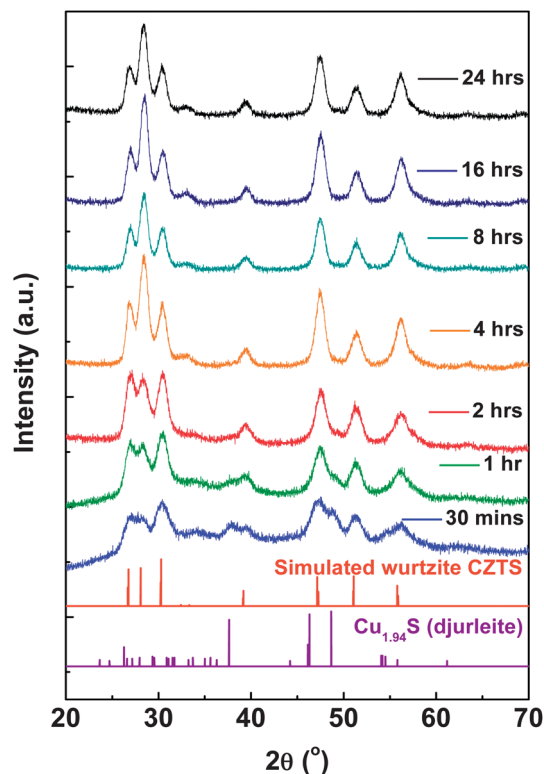


Fig. 2 XRD patterns of different nanocrystals obtained after reaction at 230 °C for different times, *i.e.* 30 minutes, 1 hour, 2 hours, 4 hours, 8 hours, 16 hours and 24 hours. Shown below these are the patterns of the starting phase djurleite $\text{Cu}_{1.94}\text{S}$ (JCPDS 23-0959) and the simulated pattern of wurtzite CZTS.

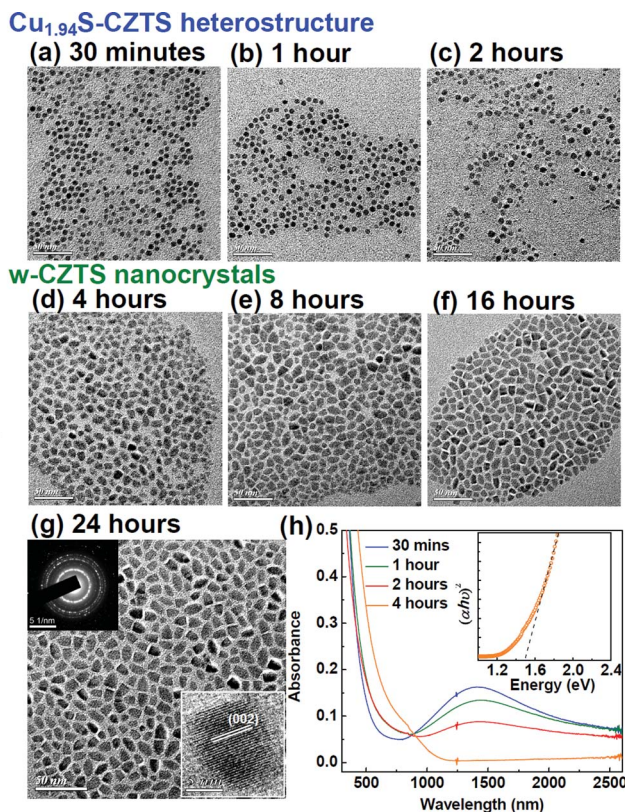


Fig. 3 (a–g) TEM images of different nanocrystals obtained after reaction at 230 °C for different reaction times. The HRTEM image and the electron diffraction pattern are shown in the inset of (g). (h) Absorption spectra of different nanocrystals obtained after reaction at 230 °C for different reaction times. The determination of the band gap of w-CZTS obtained after reaction at 230 °C for 4 hours is shown in inset.

heterostructure and bullet shaped or leaf shaped pristine w-CZTS nanocrystals that are analogous to those shown in Fig. 1c–e. The inset in Fig. 3g shows the high resolution TEM (HRTEM) image of w-CZTS with the lattice fringe of the (002) plane along the preferred orientation, which also suggests the single crystalline structure and high crystallinity of the w-CZTS nanocrystals. Additionally, Fig. 3h plots the absorption spectra of the nanocrystals synthesized at 230 °C for 30 minutes, 1 hour, 2 hours and 4 hours, which consistently further shows the diminishing of the plasmonic absorbance as the $\text{Cu}_{1.94}\text{S}$ starting phase is expelled when the reaction time reaches 4 hours. The band gap of the pristine w-CZTS (with a reaction time of longer than 4 hours) can be determined to be ~ 1.5 eV (as shown in the inset of Fig. 3h) which is close to the value for zinc blende CZTS nanocrystals.¹⁵ After the reaction at 230 °C for 24 hours (Fig. 3g), w-CZTS has dimensions of around 13 nm and a size distribution of around 15%. This size distribution is narrower than that of w-CZTS after the reaction at 260 °C for 1 hour (Fig. 1e, $\sigma_r = 28\%$). The result can be attributed to the longer reaction time leading to a size focusing effect (an effect due to the faster growth of smaller nanocrystals than larger nanocrystals).^{1,2} Moreover, the value of $\sigma_r = 15\%$ is close to that indicating monodispersity ($\sigma_r < 10\%$).¹ The uniform and homogeneous nucleation of $\text{Cu}_{1.94}\text{S}$ during heating (Fig. 1c and d and Fig. 3a and b of the

monodispersed nanoparticles) accounts for this relatively narrow size distribution. However, it is noteworthy that when the reaction proceeds for 2 hours, some broken crystals and irregularly shaped nanocrystals were observed. This phenomenon has also been observed by others with similar nanocrystal formation mechanisms.³¹ Consequently, the broken crystals slightly affect the size distribution of the obtained w-CZTS nanocrystals. To confirm all four elements are uniformly presented in the w-CZTS nanocrystals, electron energy loss spectroscopy (EELS) mapping with nanoscale resolution was performed. Fig. 4a and Fig. 4b–e show the TEM image and corresponding EELS elemental mappings of Cu, Zn, Sn and S respectively. The four elements are homogeneously distributed in each nanocrystal which suggests that the w-CZTS nanocrystals have a uniform composition without a second phase. As a short conclusion, the obtained w-CZTS nanocrystals synthesized through the one-pot heating process have highly crystalline, single crystal, single phase, uniform compositions and relatively narrow size distributions. This process takes advantage of the ease of formation of the homogeneous nucleus $\text{Cu}_{1.94}\text{S}$.

The proposed reaction mechanism to form the w-CZTS nanocrystals is further confirmed by the non-discriminative selection of tin and zinc precursors. Namely, the typical challenge of balancing the reactivity among all of the cation precursors in order to avoid a second phase or composition nonuniformity can be overcome when preparing multi-component nanocrystals through the formation of homogeneous nuclei by one cation using a simple heating reaction. In this study, the nucleation would be well controlled by the preferentially formed $\text{Cu}_{1.94}\text{S}$ nanoparticles with monodispersity. This starting phase would be completely expelled and transformed to pristine w-CZTS due to the extremely high mobility of the cations meaning that cation inter-diffusion with the surrounding anions would become very effective. We adopted different combinations of zinc and tin precursors, *i.e.* zinc chloride–tin chloride and zinc acetate–tin acetate to conduct a synthesis based on the reaction using the zinc acetate–tin chloride pair. Fig. 5a and Fig. 5b–c show the powder XRD patterns and TEM images of the obtained nanocrystals respectively. Both nanocrystals exhibited the pristine w-CZTS phase as can be seen when compared to the simulated w-CZTS patterns

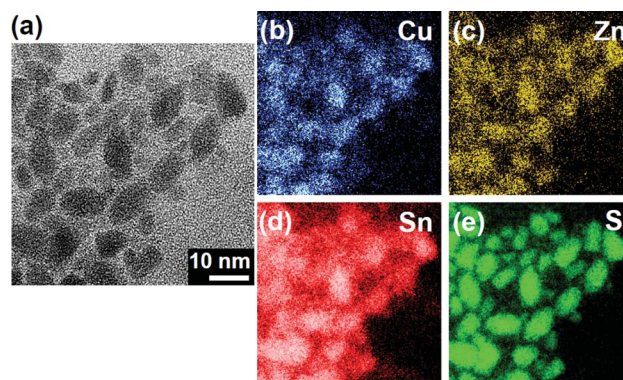


Fig. 4 TEM-EELS mapping of w-CZTS nanocrystals: (a) zero-loss mapping, (b) Cu mapping, (c) Zn mapping, (d) Sn mapping and (e) S mapping.

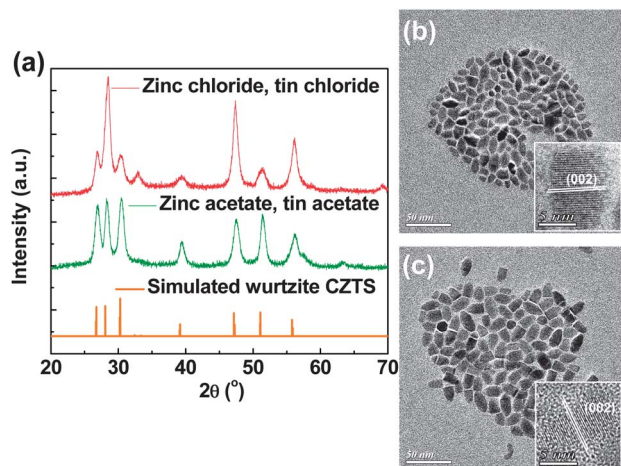


Fig. 5 (a) XRD patterns and (b–c) TEM images of CZTS nanocrystals synthesized using different combinations of zinc and tin precursors, i.e. (b) zinc chloride and tin chloride and (c) zinc acetate and tin acetate.

(ESI[†]). Moreover, the w-CZTS nanocrystals formed from the different combinations reveal similar bullet or leaf shapes to those observed in Fig. 3g. The results provide evidence that the w-CZTS formation mechanism can be universally extended to other zinc and tin precursors with a general procedure.

Conclusions

In summary, a simple one-pot heating synthesis strategy for preparing w-CZTS nanocrystals is demonstrated herein. High quality w-CZTS nanocrystals with high crystallinity, single phase, uniform spatial composition distribution, and uniform size distribution are obtained. The nanocrystal formation mechanism for the nucleation, growth and cation inter-diffusion is clearly understood. This distinctive mechanism enables non-discriminative selection of zinc and tin precursors without the complicated control of cation reactivity. The present work considerably extends the current knowledge and technology of the chemical synthesis of promising multi-component nanocrystals which can be easily scaled up for practical applications.

Acknowledgements

Financial support obtained from the National Science Council of Taiwan (100-2120-M-002-007 and 100-3113-E-002-012) and the Institute of Nuclear Energy Research (Projects 10120011NER030) are highly appreciated.

Notes and references

- S. G. Kwon and T. Hyeon, *Small*, 2011, **7**, 2685.
- X. Peng, J. Wickham and A. P. Alivisatos, *J. Am. Chem. Soc.*, 1998, **120**, 5343.
- C. B. Murray, D. J. Norris and M. G. Bawendi, *J. Am. Chem. Soc.*, 1993, **115**, 8706.
- D. V. Talapin, A. L. Rogach, A. Kornowski, M. Haase and H. Weller, *Nano Lett.*, 2001, **1**, 207.
- S. G. Kwon and T. Hyeon, *Acc. Chem. Res.*, 2008, **41**, 1696.
- N. R. Jana and X. Peng, *J. Am. Chem. Soc.*, 2003, **125**, 14280.
- S. H. Choi, K. An, E. G. Kim, J. H. Yu, J. H. Kim and T. Hyeon, *Adv. Funct. Mater.*, 2009, **19**, 1645.
- Y. Chen, E. Johnson and X. Peng, *J. Am. Chem. Soc.*, 2007, **129**, 10937.
- J. Park, K. An, Y. Hwang, J. G. Park, H. J. Noh, J. Y. Kim, J. H. Park, N. M. Hwang and T. Hyeon, *Nat. Mater.*, 2004, **3**, 891.
- W. S. Seo, H. H. Jo, K. Lee and J. T. Park, *Adv. Mater.*, 2003, **15**, 795.
- J. Joo, H. B. Na, T. Yu, J. H. Yu, Y. W. Kim, F. Wu, J. Z. Zhang and T. Hyeon, *J. Am. Chem. Soc.*, 2003, **125**, 11100.
- L. Tian and J. J. Vittal, *New J. Chem.*, 2007, **31**, 2083.
- C. Zou, L. Zhang, D. Lin, Y. Yang, Q. Li, X. Xu, X. Chen and S. Huang, *CrystEngComm*, 2011, **13**, 3310.
- S. Shen, Y. Zhang, L. Peng, B. Xu, Y. Du, M. Deng, H. Xu and Q. Wang, *CrystEngComm*, 2011, **13**, 4572.
- Q. Guo, H. W. Hillhouse and R. Agrawal, *J. Am. Chem. Soc.*, 2009, **131**, 11672.
- C. Steinhagen, M. G. Panthani, V. Akhavan, B. Goodfellow, B. Koo and B. A. Korgel, *J. Am. Chem. Soc.*, 2009, **131**, 12554.
- S. C. Riha, B. A. Parkinson and A. L. Prieto, *J. Am. Chem. Soc.*, 2009, **131**, 12054.
- Q. Guo, G. M. Ford, W. C. Yang, B. C. Walker, E. A. Stach, H. W. Hillhouse and R. Agrawal, *J. Am. Chem. Soc.*, 2010, **132**, 17384.
- T. K. Todorov, K. B. Reuter and D. B. Mitzi, *Adv. Mater.*, 2010, **22**, E156.
- X. Lu, Z. Zhuang, Q. Peng and Y. Li, *Chem. Commun.*, 2011, **47**, 3141.
- A. Singh, H. Geaney, F. Laffir and K. M. Ryan, *J. Am. Chem. Soc.*, 2012, **134**, 2910.
- S. Chen, A. Walsh, Y. Luo, J. H. Yang, X. G. Gong and S. H. Wei, *Phys. Rev. B: Condens. Matter*, 2010, **82**, 195203.
- Y. Zhao and C. Burda, *Energy Environ. Sci.*, 2012, **5**, 5564.
- H. Jiang, P. Dai, Z. Feng, W. Fan and J. Zhan, *J. Mater. Chem.*, 2012, **22**, 7502.
- J. J. Wang, J. S. Hu, Y. G. Guo and L. J. Wan, *NPG Asia Materials*, 2012, **4**, e2.
- R. Xie, M. Rutherford and X. Peng, *J. Am. Chem. Soc.*, 2009, **131**, 5691.
- J. M. Luther, P. K. Jain, T. Ewers and A. P. Alivisatos, *Nat. Mater.*, 2011, **10**, 361.
- I. Kriegel, C. Jiang, J. Rodríguez-Fernández, R. D. Schaller, D. V. Talapin, E. da Como and J. Feldmann, *J. Am. Chem. Soc.*, 2012, **134**, 1583.
- S. A. Maier, *Plasmonics: Fundamentals and Applications*, 2007, p. 65.
- S. T. Connor, C. M. Hsu, B. D. Weil, S. Aloni and Y. Cui, *J. Am. Chem. Soc.*, 2009, **131**, 4962.
- W. Han, L. Yi, N. Zhao, A. Tang, M. Gao and Z. Tang, *J. Am. Chem. Soc.*, 2008, **130**, 13152.
- J. Y. Chang and C. Y. Cheng, *Chem. Commun.*, 2011, **47**, 9089.
- M. Kruszynska, H. Borchert, J. Parisi and J. Kolny-Olesiak, *J. Am. Chem. Soc.*, 2010, **132**, 15976.
- S. H. Choi, E. G. Kim and T. Hyeon, *J. Am. Chem. Soc.*, 2006, **128**, 2520.